Optimized pulse width modulation pattern strategy for three-dimensional profilometry with projector defocusing

Chao Zuo,[1,2,*] Qian Chen,[1,2] Shijie Feng,[1] Fangxiaoyu Feng,[1] Guohua Gu,[1] and Xiubao Sui[1]

[1]Jiangsu Key Laboratory of Spectral Imaging & Intelligence Sense, Nanjing University of Science and Technology, Nanjing, Jiangsu Province 210094, China

[2]Key Laboratory of Photoelectronic Imaging Technology and System, Ministry of Education of China, Beijing Institute of Technology, Beijing 100081, China

*Corresponding author: surpasszuo@163.com

Received 21 March 2012; revised 11 May 2012; accepted 12 May 2012; posted 14 May 2012 (Doc. ID 165151); published 29 June 2012

Three-dimensional profilometry by sinusoidal fringe projection using phase-shifting algorithms is usually distorted by the nonlinear intensity response of commercial video projectors. To overcome this problem, several methods including sinusoidal pulse width modulation (SPWM) were proposed to generate sinusoidal fringe patterns with binary ones by defocusing the project to some certain extent. However, the residual errors are usually nonnegligible for highly accurate measurement fields, especially when the defocusing level is insufficient. In this work, we propose two novel methods to further improve the defocusing technique. We find that by properly optimizing SPWM patterns according to some criteria, and combining SPWM technique with four-step phase-shifting algorithm, the dominant undesired harmonics will have no impact on the phase obtained. We also propose a new sinusoidal fringe generation technique called tripolar SPWM, which can generate ideal sinusoidal fringe patterns with a very small degree of defocusing. Simulations and experiments are presented to verify the performance of these two proposed techniques.

OCIS codes: 120.0120, 120.2650, 100.5070, 120.5050.

1. Introduction

Optical noncontact three-dimensional (3D) shape measurement techniques have been employed for several years to measure the 3D profile of objects. With the recent advancement in digital display devices such as liquid crystal displays (LCDs) and digital mirror devices (DMDs), 3D shape measurement based on digital fringe projection has been rapidly expanding [1–4]. It is much easier and more convenient to generate and control the fringe patterns with a commercial video projector. However, due to the nonlinear response of the projection engines of projectors [5–7], it remains a challenging task to develop a high-speed 3D imaging system with an off-the-shelf projector. Projector response calibration is usually needed to perform high-quality 3D shape measurement using a digital fringe projection and phase-shifting method. Unfortunately, the intensity response of a projector actually changes with the time lapse [8,9]. So this nonlinearity problem cannot be solved by one-time calibration methods such as projection of predistorted patterns [10], creation of a lookup table for error compensation [11], and use of a calibration board [12]. To overcome this problem, techniques that generate sinusoidal fringe patterns by using a binary pattern are proposed to elude

1559-128X/12/194477-14$15.00/0

the nonlinearity problem. Ayubi *et al.* [8] partitioned a sinusoidal fringe pattern into a temporal sequence of binary fringes and acquired the binarized images to reproduce an ideal sinusoidal fringe pattern. This technique was recently improved by encoding the binary pattern in three-color channels [13]. However, it still requires at least nine images for 8 bit shape profiling, which reduces the measurement speed. Besides, the coding errors resulting from the out-of-focus blur limit its measurement depth range. In contrast, another class of techniques generates sinusoidal fringe patterns by rationally defocusing a binary pattern. Su *et al.* [14] introduced a technique for defocusing a square wave generated by the Ronchi grating for 3D shape measurement. Lei and Zhang [9] proposed a technique called squared binary defocusing method (SBM) that is to generate sinusoidal fringe patterns by properly defocusing squared binary structured ones using a digital video projector. Ayubi *et al.* [15] presented methods for generating the binary pattern by the sinusoidal pulse width modulation (SPWM) technique of electrical engineering. Wang and Zhang proposed a binary pattern generation technique called optimal pulse width modulation (OPWM) [16] and conduct a comparative study on SBM, SPWM, and OPWM [17]. Compared to SBM, the SPWM and OPWM methods can produce better 3D shape measurement results especially when the defocusing degree is small. But the phase error caused by some unwanted high-order harmonics of the generated patterns of SPWM and OPWM methods is still nonnegligible, especially when the project is nearly focused [17]. The trade-off between defocusing degree and pattern contrast results in narrow depth of field of the measurement system.

The purpose of the present paper is to further improve the defocusing technique in the following two ways. Specifically, first the SPWM technique is optimized, combining the four-step phase-shifting technique; the dominant error-causing harmonics can be shifted to higher even multiplies of fundamental frequency, and thus they have no impact on calculated phase. Second, we propose a technique called tripolar SPWM, in which the undesired harmonics can be displaced so far away from the fundamental frequency that ideal sinusoidal patterns can be generated with very small defocusing level. Both simulation and experimental results showed that, with the proposed methods, high measurement accuracy can be achieved with conventional three- or four-step phase-shifting algorithms even using a small degree of defocusing.

2. Principle

A. Digital Fringe Projection Profilometry

A crossed-optical-axes triangulation is usually utilized in the digital fringe projection profilometry as shown in Fig. 1. Points P and C are the centers of the entrance pupil of CCD, and the exit pupil of the projector and the lines PO and CO are the optical axis of the projector and the CCD camera, respectively. The normal of this reference plane is parallel with the line CO. A sinusoidal fringe pattern generated by the projector is projected onto the measured object. For the sake of simplicity, the pattern we used only varies with the x coordinate. The distorted fringe distribution, denoted as $I(x,y)$, captured by the CCD camera is

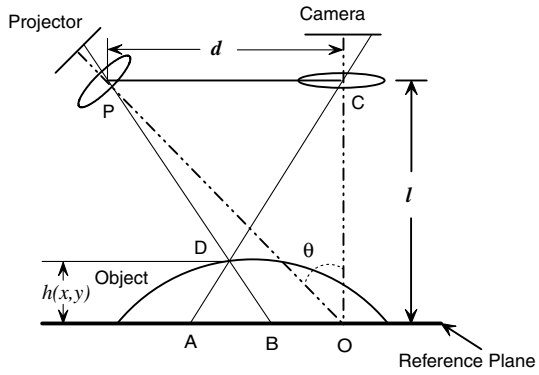

Fig. 1. Typical crossed-optical-axes profilometry arrangement.

$$I(x,y) = A(x,y) + B(x,y)\cos[\phi(x,y) + 2\pi f x], \quad (1)$$

where f is the spatial frequency of the fringe on the reference plane, $A(x,y)$ is the average intensity, $B(x,y)$ is the intensity modulation, and $\phi(x,y)$ is the phase distribution that is corresponding with the surface profile of the measured object. The relationship between the phase and surface profile can be given as

$$h(x,y) = l\phi_{AB}/[2\pi df + \phi_{AB}], \quad (2)$$

where ϕ_{AB} is the phase difference of the fringe between point A and point B, l is the distance from the entrance pupil of the CCD camera to the reference plane, and d is the distance between the entrance pupil of the CCD and the exit pupil of the projector. Once the parameters mentioned in Eq. (2) are obtained, the surface profile $h(x,y)$ can be calculated.

B. Defocusing Theory

However, the traditional digital fringe projection profilometry is not trouble-free. One of the major problems is the projector's nonlinear gamma response. This is because the commercial video projector is usually a nonlinear device that is purposely designed to compensate for human vision. This nonlinear response will result in nonsinusoidal waveforms if no compensation is used. Generally, the defocusing technique is to use computer generated binary structured images, and defocus the projector to make them become sinusoidal structured ones. The intensity of the normalized squared binary structured patterns can be represented as

$$p(x) = \mathrm{rect}\left(\frac{2x}{T}\right) * \mathrm{comb}\left(\frac{x}{T}\right), \tag{3}$$

where T is the fringe period, and $*$ stands for convolution operation. Because the structured patterns have horizontal/vertical stripes with exactly the same structure, in order to understand how the binary pattern changes when the projector is defocused, we only need to study how one horizontal cross section of the pattern alters. The Fourier transform of $p(x)$ is

$$P(f_x) = C \sum_{j=-\infty}^{+\infty} \mathrm{sinc}\left(\frac{f_x}{2f_0}\right) \cdot \delta(f_x - jf_0), \tag{4}$$

where C is a constant, and $f_0 = \frac{1}{T}$ represents the spatial frequency of the pattern. The amplitude of the harmonics of frequency is shown in Fig. 2. It can be seen that SBM produces a monotonically decaying harmonic distortion spectrum and the nonzero frequency components all exist in the odd-order harmonics.

The defocusing effect can be modeled as the convolution of a sharp image with the point spread function (PSF). The PSF is usually approximated by a circular Gaussian function [16,17],

$$h(x,y) = \frac{1}{2\pi\sigma^2} \exp\left(-\frac{x^2+y^2}{2\sigma^2}\right), \tag{5}$$

where the standard deviation σ is proportional to defocusing levels. The defocused optical system is equivalent to a spatial two-dimensional (2D) low-pass filter, which could attenuate the higher-older harmonics in SBM. But since the spectrum of SBM contains all odd-order harmonics, the projector must be properly defocused, so that the higher odd-order harmonics can be filtered out effectively and thus the ideal sinusoidal fringe can be generated. But proper defocusing is not very easy to achieve, especially when the fringe width is large. A low level of defocusing cannot remove higher-order harmonic components effectively, while a high level of defocusing will reduce the pattern contrast considerably.

C. Frequency Spectra of SPWM Waveforms

The SPWM technique is proposed in [15] to generate a high-quality sinusoidal pattern with a smaller defocusing level. Figure 3 gives an example to better illustrate its principle. The output binary patterns are modulated by comparing the desired sinusoidal pattern with a high-frequency triangular carrier [18]. When the intensity value of the sinusoidal waveform is greater than the triangular waveform, the value of SPWM pattern is "1"; otherwise, the intensity value is "0."

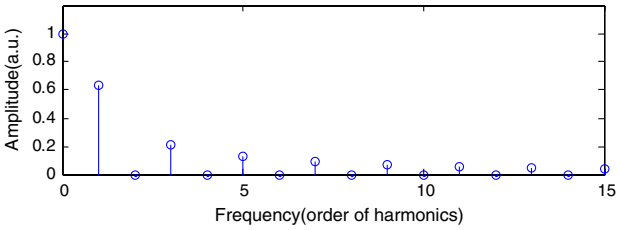

Fig. 2. (Color online) Frequency spectrum of one cross section of the squared binary structured pattern.

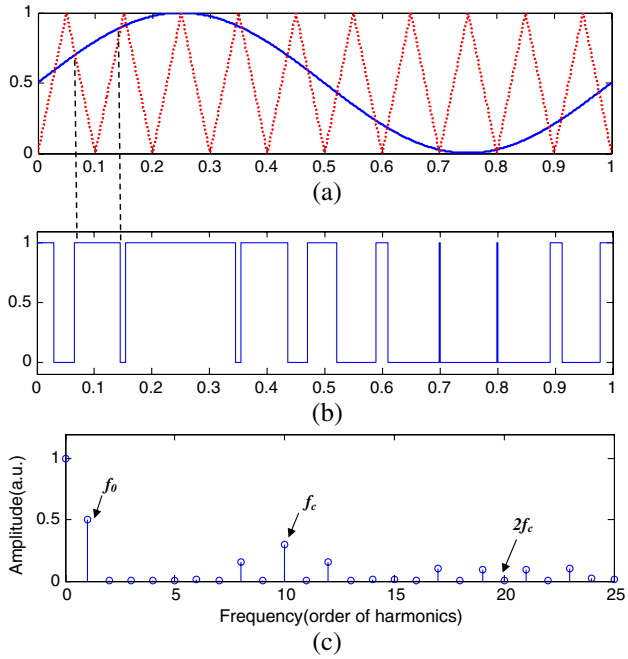

Fig. 3. (Color online) SPWM waveform generation and harmonics distribution. (a) The sinusoidal and the modulation triangle waveforms with $f_c = 10f_0$;(b) the resultant binary SPWM waveform; (c) frequency spectrum of (b).

In the spectrum of the SPWM pattern, the high-frequency harmonics are shifted farther away from the fundamental frequency and thus are easier to be suppressed with a smaller defocusing level. Ideally, the harmonics in the spectrum of the SPWM pattern includes

$$nf_c \pm kf_0. \tag{6}$$

When $n = 1,3,5,\ldots$, $k = 0,2,4,\ldots$; when $n = 2,4,6,\ldots$, $k = 1,3,5,\ldots$. Figure 3(b) shows the ideal SPWM pattern obtained with $f_c = 10f_0$, and its frequency spectrum is shown in Fig. 3(c). It can be seen that among these harmonics, the predominant spectra components occur at the carrier frequency f_c and its two side-band components spaced by $2f_0$ from f_c. The peaks around the frequency $2f_c$ do not induce noticeable phase error since their amplitudes are relatively low and their frequencies are so high that they can be easily suppressed even with a nearly focused optical system. It should be also noticed that in practice, due to the discrete nature of the generated fringe patterns, the harmonics in the spectrum of the SPWM patterns are much more complicated. This problem will be discussed at length in Section 3.

D. Sensitivity to Harmonics for Different Phase-Shifting Algorithms

In general, an N-step phase-shifting algorithm with equal phase shifts can be described as

$$I_n(x,y) = A(x,y) + B(x,y)\cos[\phi(x,y) + 2\pi n/N], \quad (7)$$

where $A(x,y)$ is the average intensity, $B(x,y)$ is the intensity modulation, $\phi(x,y)$ is the phase to be solved for, n is phase-shift index, and $n = 1, 2, 3, \ldots, N$. Solving these equations leads to

$$\phi(x,y) = \tan^{-1}\frac{\sum_{n=1}^{N} I_n(x,y)\sin(2\pi n/N)}{\sum_{n=1}^{N} I_n(x,y)\cos(2\pi n/N)}. \quad (8)$$

Suppose we have a group of phase-shifted sinusoid waveforms, mixed with high-order harmonics, defined as

$$I'_n(x,y) = A(x,y) + B(x,y)[\cos\,\phi(x,y) + 2\pi n/N] + \sum_{k=2}^{\infty} B_k(x,y)\{\cos\,k[\phi(x,y) + 2\pi n/N]\}. \quad (9)$$

$B(x,y)\cos[\phi(x,y) + 2\pi n/N]$ is the main signal, and $\sum_{k=2}^{\infty} B_k(x,y)\{\cos\,k[\phi(x,y) + 2\pi n/N]\}$ are the harmonics terms. When we still apply Eq. (8) to compute the desired phase of fundamental signal, a harmonics distorted phase will be obtained as $\phi'(x,y)$.

To analyze how each harmonic frequency component affects the calculated phase for different phase-shifting algorithms, we just added one specific harmonic component to the ideal sinusoid wave signals one time. Then we compared the calculated phase $\phi'(x,y)$ with the correct one $\phi(x,y)$, and we would know whether we can get a distortion-free phase even when the particular harmonic component exists. Table 1 summarizes the results.

A key regulation can be observed from the table that N-step phase-shifting is only sensitive to the presence of the $(p+1)N \pm 1$th harmonics, where p is an integer. For example, the six-step algorithm is insensitive to harmonics 2, 3, and 4, but also to harmonics 6, 8, 9, 10, 12, 14 . . . . It is sensitive only to harmonics $5 + 6p$ and $7 + 6p$.

E. OPWM and Large-Step Binary Phase-Shifting Algorithms

More recently, Wang and Zhang [16] proposed a binary pattern scheme called OPWM, which could selectively eliminate some specific undesired frequency components in the spectra of SBM patterns. Since there are only odd-order harmonics components in the spectrum of the SBM pattern, and according to Table 1, three-step phase-shifting is insensitive to triplen harmonics, the fifth-order and seventh-order harmonics are the dominant phase error sources. The OPWM technique can selectively eliminate these frequency components by inserting different types of notches in an SBM pattern. Experimental results show it can effectively reduce the phase error in three-step phase-shifting with a slightly defocused projector. However, for the even-step phase-shifting method, e.g., four-step phase-shifting, more harmonics need to be eliminated to achieve a good measurement quality, and it is impractical to eliminate too many harmonics for the OPWM technique due to the discrete fringe generation nature.

Ekstrand and Zhang [19] use the seven-step or nine-step binary phase-shifting algorithm to produce accurate 3D measurements with a nearly focused projector. From Table 1 and the above discussion, it can be deduced that the seven-step phase-shifting algorithm is sensitive only to $6 + 7p$- and $9 + 7p$-order harmonics, and the nine-step phase-shifting algorithm is sensitive only to $8 + 9p$- and $10 + 9p$-order harmonics. For SBM patterns whose spectrums contain only odd-order harmonics, the nine-step phase-shifting algorithm does not experience any error from harmonics below the 17th order. Therefore, the remaining harmonic induced errors are negligible with nearly focused binary patterns. However, this improvement is achieved at the cost of prolonging the acquisition time, since many more fringe patterns are needed.

3. Proposed Methods

A. SPWM Plus Four-Step Phase-Shifting Algorithm

It is not difficult to understand that two factors should be considered when using phase-shifting profilometry with nonsinusoidal patterns: (1) the spectrum/harmonics of the fringe pattern; (2) the

Table 1. Sensitivity of Different Phase-Shifting Algorithms to Harmonics

	Harmonics																
Number of Step	2	3	4	5	6	7	8	9	10	11	12	13	14	15	16	17	18
3	×		×	×		×	×		×	×		×	×		×	×	
4		×		×		×		×		×		×		×		×	
5			×		×			×		×			×		×		
6				×		×				×		×				×	
7					×		×					×		×			
8						×		×						×		×	
9							×		×							×	

sensitivity to harmonics of the phase-shifting algorithm. In general, the more steps of phase-shifting employed, the better the harmonics resistant ability will be. According to the regulation summarized in Table 1, we know that an $n+2$ step phase-shifting algorithm could retrieve phase accurately from fringe patterns with harmonics up to the nth order. Besides, one can seldom observe harmonics higher than 15th order in a practical profilometry system due to the inherent blurring effect of the optical device. So when the number of phase steps is large enough, we do not have to consider the spectrum/harmonics of the designed pattern. And conversely, if the sinusoidality of the patterns is good enough, three-step phase-shifting will be sufficient to obtain satisfactory results. However, in the spectrum of a SPWM pattern, the harmonics at the carrier frequency f_c and its two side-band components spaced by $2f_0$ cannot be neglected, especially when the projector is nearly focused. Besides, we want to use fewer steps of phase-shifting for fast measurements. So the two factors should be considered simultaneously.

From Table 1, it can be found that the prominent characteristic of the four-step phase-shifting algorithm is that it is insensitive to all even-order harmonics. On the other hand, from Eq. (6), we know that if the frequency of the triangle carrier is even multiples of the fundamental frequency, the predominant harmonics components (f_c and its two side-band components occur at $f_c \pm 2f_0$) are all even-order harmonics. So these harmonic components do not induce phase error in four-step phase-shifting algorithm. One consequence of this is that all even-order harmonics have no impact on phase, leaving other odd-order harmonics to dominate. Although the peaks around the frequency $2f_c$ are odd-order harmonics, their frequencies are very high and can be easily suppressed even with a nearly focused optical system. Considering these two aspects, we can combine the SPWM technique with the four-step phase-shifting algorithm.

It must be also mentioned that the above analysis is under ideal conditions. In practical applications, the projected pattern consists of only digital discrete pixels, and the number of sampling points in each period is limited. The harmonics distribution of the real SPWM pattern is much more complex. In general, the harmonic components in the discrete patterns are more than those under ideal conditions. Sometimes, even some low-order harmonics may spring up. To minimize the error caused by the discrete nature of the pattern, the following principles are recommended when designing the SPWM pattern.

Principle 1: The fringe period should be properly chosen to avoid phase-shift error. For the four-step phase-shifting algorithm, the fringe width should be a multiple of 4. When designing the SPWM pattern, to ensure each period of the waveform is identical, design one-period pattern first, and then extend it to the full size. Finally, the phase-shifting is realized by spatially moving the binary patterns. For example, a $\pi/2$ phase-shifting can be realized by moving 1/4 period of the SPWM pattern.

Principle 2: There are two ways to generate the discrete SPWM pattern. To better explain, we illustrate these two methods in Fig. 4. Suppose we want to generate a SPWM pattern with a fringe pitch of 80 pixels and $f_c = 10f_0$; we can first discretize one period of the sinusoidal waveform and the triangular waveform to 80 pixels [Fig. 4(a)] and then compare their intensity values to get the final SPWM pattern [Fig. 4(c)]. Another way is to generate one period of the sinusoidal waveform and the triangular waveform with a much higher sample rate and get the

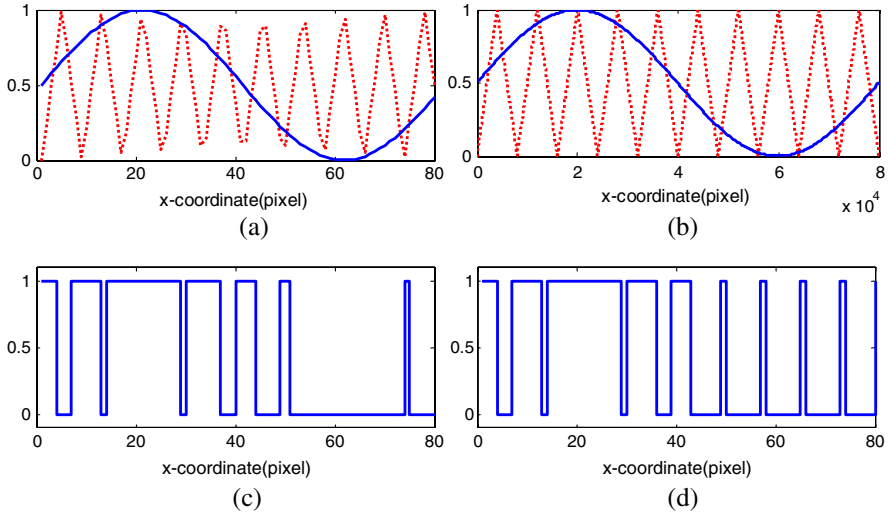

Fig. 4. (Color online) Comparison between two ways to generate discrete SPWM pattern with fringe pitch of 80 pixels and $f_c = 10f_0$. (a) The sinusoidal and the modulation triangle waveforms with low resolution; (b) the sinusoidal and the modulation triangle waveforms with high resolution; (c) the resultant SPWM pattern from (a); (d) the resultant SPWM pattern by down sampling the high resolution SPWM pattern obtained from (b).

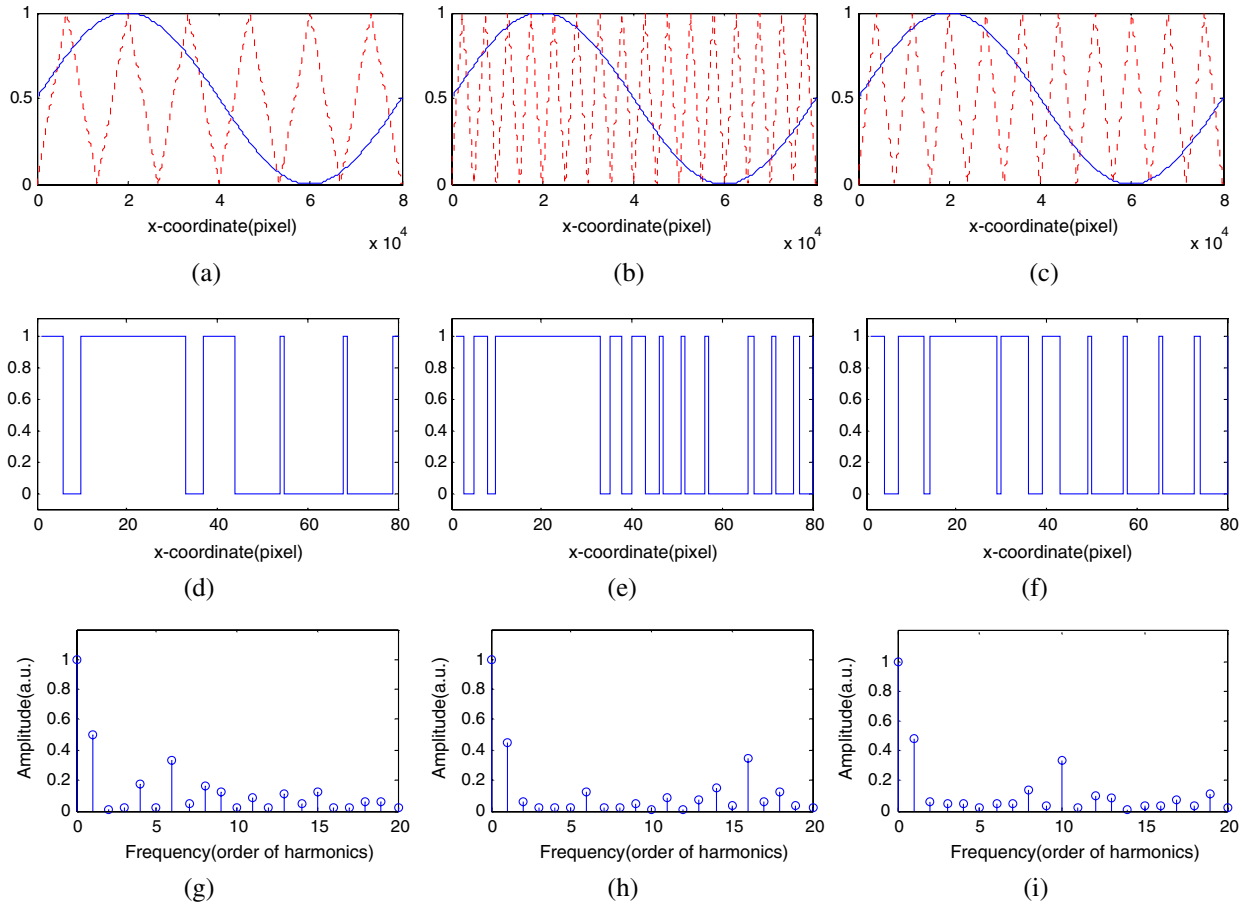

Fig. 5. (Color online) Comparison among SPWM patterns (fringe pitch 80 pixels) with different modulation frequencies. Top row: The sinusoidal and the modulation triangle waveforms with (a) $f_c = 6f_0$, (b) $f_c = 12f_0$, and (c) $f_c = 10f_0$. Middle row: (d)–(f) the resultant binary SPWM waveform from (a), (b), and (c). Bottom row: (g)–(i) frequency spectra of (d), (e), and (f).

high-resolution SPWM pattern [we use 80,000 points in Fig. 4(b)], and then we subsample the high-resolution SPWM pattern to get the final SPWM pattern with the fringe pitch we want [Fig. 4(d)]. It is obvious that the triangular waveform in Fig. 4(a) is seriously distorted due to the inadequate sampling rate, while the SPWM pattern generated by the second approach has a better shape and symmetry. Besides, the second method that subsampling an ideal, high-resolution SPWM pattern to get the final low-resolution one is more theoretically understandable.

Principle 3: Since the ideal SPWM pattern is binary, its spectrum width is infinite. The spectrum aliasing problem is inevitable for the discrete SPWM pattern. To reduce the spectrum aliasing effect, (1) f_c should be properly selected, neither too great nor too small. Figure 5 shows three SPWM patterns with different f_c and their spectra. If the f_c is too small, the peaks around the frequency $2f_c$ cannot be effectively shifted to higher frequencies. On the other hand, when the f_c is too large, some low-order or error-causing odd-order harmonics will appear due to the spectrum aliasing. (2) Remove the spikes

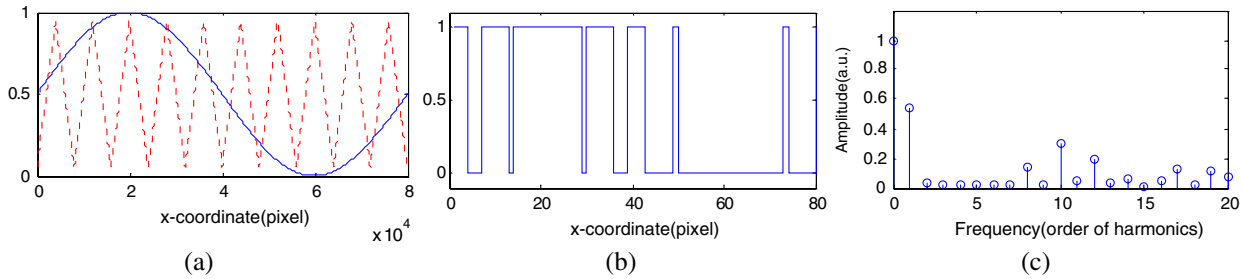

Fig. 6. (Color online) Alleviating the aliasing effect by reducing the amplitude of the triangle carrier by 3%. (a) The sinusoidal and the modulation triangle waveforms with reduced amplitude; (b) the resultant binary SPWM waveform; (c) frequency spectrum of (b). Comparing with the frequency spectrum shown in Fig. 5(f), the improvement is obvious.

with small width in the discrete SPWM pattern by reducing the amplitude of the triangle carrier. The spikes in SPWM waveform will induce large high-frequency components in its spectrum, which will aggravate the spectrum aliasing problem. Figure 6 gives an example that further optimizes the pattern shown in Fig. 5(f) by reducing the amplitude of the triangle carrier by 3%. Figure 6(b) shows the final waveform, and Fig. 6(c) shows its spectrum. It is evident that the undesired harmonics are significantly reduced and the spectrum is very close to the ideal case.

Therefore, the above three aspects must be taken into account when one wants to design a good discrete SPWM pattern. In Fig. 7, we give two more good examples of SPWM patterns generated by using the above rules. The fringe pitch of Fig. 7(a) is 60 pixels, and f_c is chosen as $8f_0$. The fringe pitch of Fig. 7(c) is 100 pixels, and f_c is chosen as $12f_0$.

B. Tripolar SPWM

By combining the SPWM technique with the four-step phase-shifting algorithm, we can effectively elude the negative effect of some high-order harmonic on phase. But generally, we still prefer that the defocused pattern can be produced as sinusoidally as possible so that phase-shifting algorithms with any steps can be applied without considering their harmonics sensitivity.

The SPWM referred before adopts only two gray-levels (i.e., 0 and 1), so it can also be called bipolar SPWM or two-level SPWM. If we introduce one more gray-scale (i.e., 0.5), there will be three gray-levels in the SPWM waveform. This additional gray-scale provides more possibilities of improving the sinusoidality of the defocused pattern. Besides, since only three kinds of gray-scales are used, the intensity

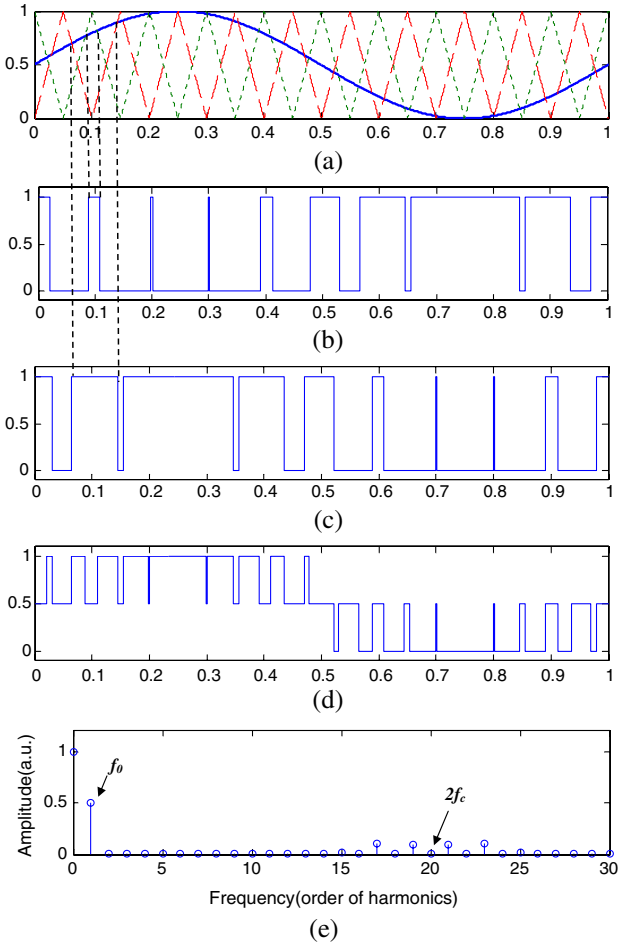

Fig. 8. (Color online) Tripolar SPWM wave form generation and harmonics distribution. (a) The sinusoidal and the two modulation triangle waveforms displaced by $\pi(f_c = 10f_0)$; (b),(c) the two binary SPWM waveforms obtained; (d) the resultant tripolar SPWM pattern; (e) frequency spectrum of (d).

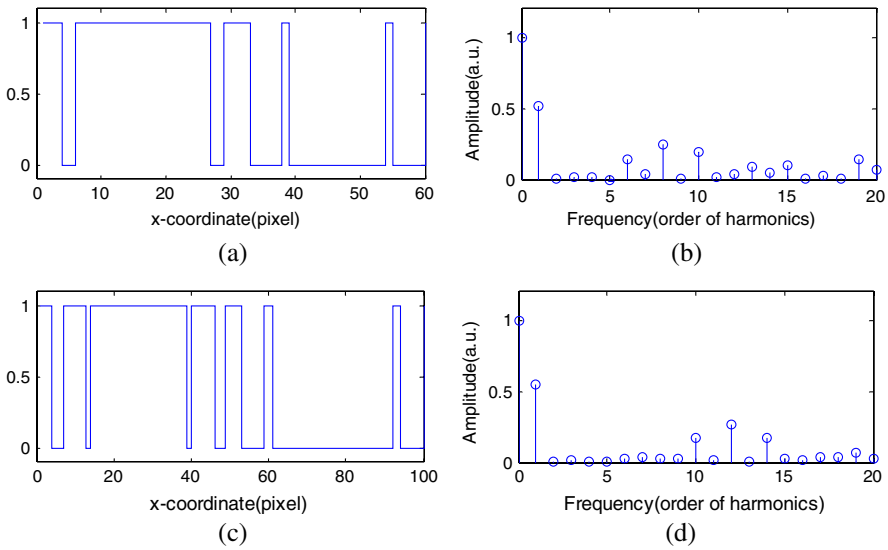

Fig. 7. (Color online) Two good examples of SPWM patterns generated using the proposed rules. (a) The binary SPWM waveform with fringe pitch of 60 pixels and $f_c = 8f_0$; (b) frequency spectrum of (a); (c) the binary SPWM waveform with fringe pitch of 100 pixels and $f_c = 12f_0$; (b) frequency spectrum of (c).

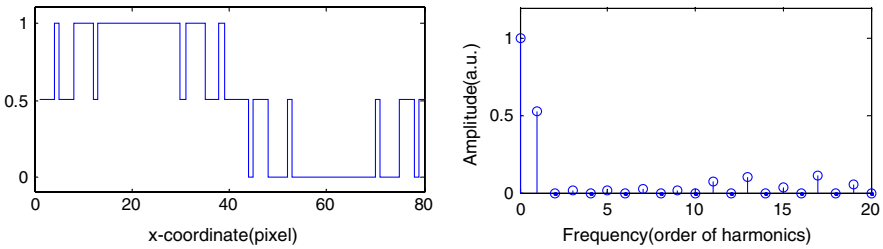

Fig. 9. (Color online) A good example of tripolar SPWM pattern generated using the proposed optimization rules. (a) The tripolar SPWM waveform with fringe pitch of 80 pixels and $f_c = 8f_0$; (b) frequency spectrum of (a).

calibration is a very easy job. We call this three-gray-level SPWM technique tripolar SPWM.

Figure 8 shows how the tripolar SPWM pattern is generated ($f_c = 10f_0$). First, two high-frequency triangular carriers displaced by π shift in phase are compared with desired a sinusoidal pattern to get two bipolar SPWM patterns. Note the second bipolar SPWM pattern corresponding to the π shifted triangular carrier (shown in red) should be inversed; i.e., when the intensity value of the sinusoidal waveform is less than the triangular waveform, the value of SPWM pattern is "1"; otherwise, the intensity value is "0." Then the resultant tripolar SPWM waveform is the difference of the two bipolar SPWM patterns [18].

The harmonics in the spectrum of the tripolar SPWM pattern includes

$$2nf_c \pm kf_0, \tag{10}$$

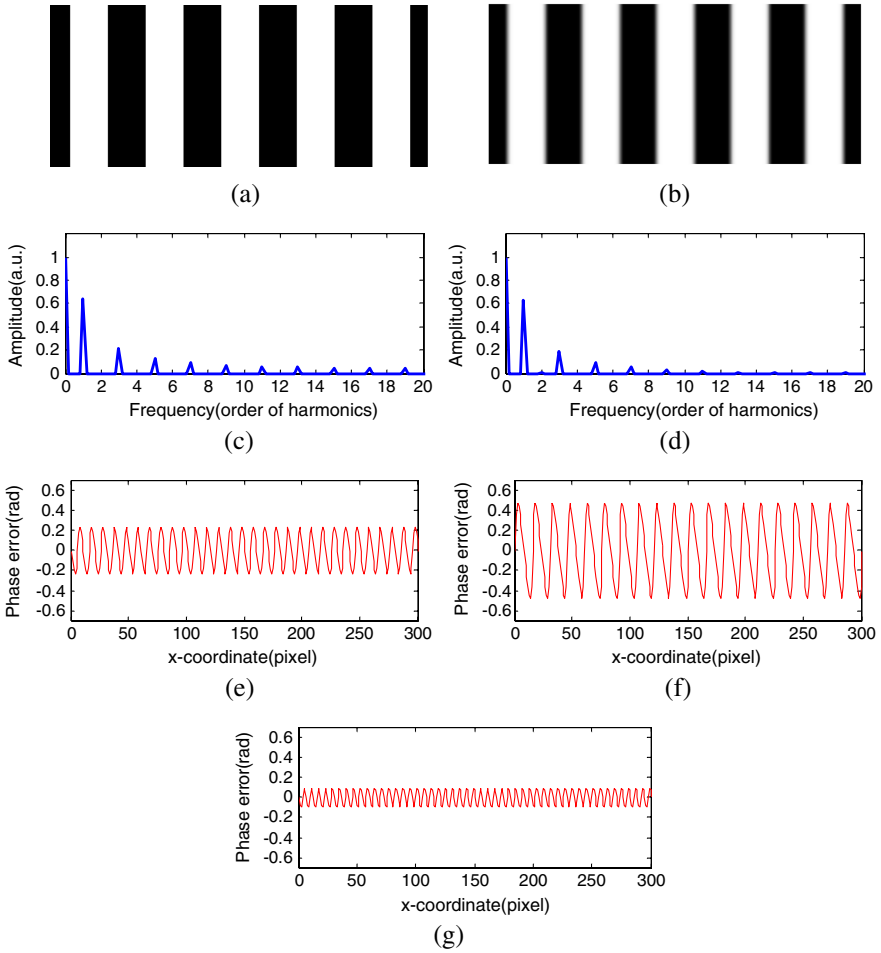

Fig. 10. (Color online) Simulation results of SBM using three to five-step phase-shifting algorithms. (a) The original squared binary structured pattern; (b) the Gaussian smoothed version of (a); (c) frequency spectrum of (a); (d) frequency spectrum of (b); (e) the phase error of three-step algorithm (RMS: 0.1638 rad); (f) the phase error of four-step algorithm (RMS: 0.3250 rad); (g) the phase error of five-step algorithm (RMS: 0.0697 rad).

where $n = 1, 2, 3, \ldots$, $k = 1, 3$. In general, when n is greater than or equal to 2, the harmonics can be neglected since their orders are too high. Figure 8(e) shows the spectrum of the tripolar SPWM waveform shown in Fig. 8(d). It can be observed that the spectrum of the tripolar SPWM pattern has peaks around the frequency $2f_c$, locating at $2f_c \pm f_0$, $2f_c \pm 3f_0$. The order of these harmonics is beyond 16, so they can be easily suppressed even with a nearly focused optical system, and thus an ideal sinusoidal pattern can be obtained.

It is worthwhile to note that when designing the tripolar SPWM patterns, the three principles given in Section 3.A are also applicable. Figure 9 shows a good example of the tripolar SPWM pattern generated according to these rules. The f_c is chosen as $7f_0$, and the fringe pitch is 80 pixels.

4. Simulations

Simulations were carried out to verify the effectiveness of the proposed methods. In this research, a Gaussian filter with a size of 8 pixels and a standard deviation of 1.5 pixels was applied for patterns generated by different methods to approximate the slightly defocusing effect. We compared the phase errors in the different pattern schemes for three-, four-, and five-step phase-shifting algorithms and chose the fringe pitch as 60 pixels to avoid phase-shift error. The phase was directly calculated from the fringe patterns, so the ideal unwrapped phase should be a perfect slope. The phase errors were computed by subtracting the unwrapped phase by the ideal slope.

Figure 10(a) shows the SBM pattern, and Fig. 10(b) shows its defocused version. Since the standard deviation of Gaussian filter applied was rather small, the shape of the SBM pattern was not changed so much. The spectra of the two patterns are shown in Figs. 10(c) and 10(d), respectively. It can be seen that the harmonics higher than 13th order have been effectively suppressed by the filter. The phase error curves and their root-mean-square (RMS) values obtained by three-, four-, and five-step phase-shifting algorithms are shown in Figs. 10(e), 10(f), and 10(g), respectively. The spectrum shown in Fig. 10(d), together with Table 1, was carefully examined to better

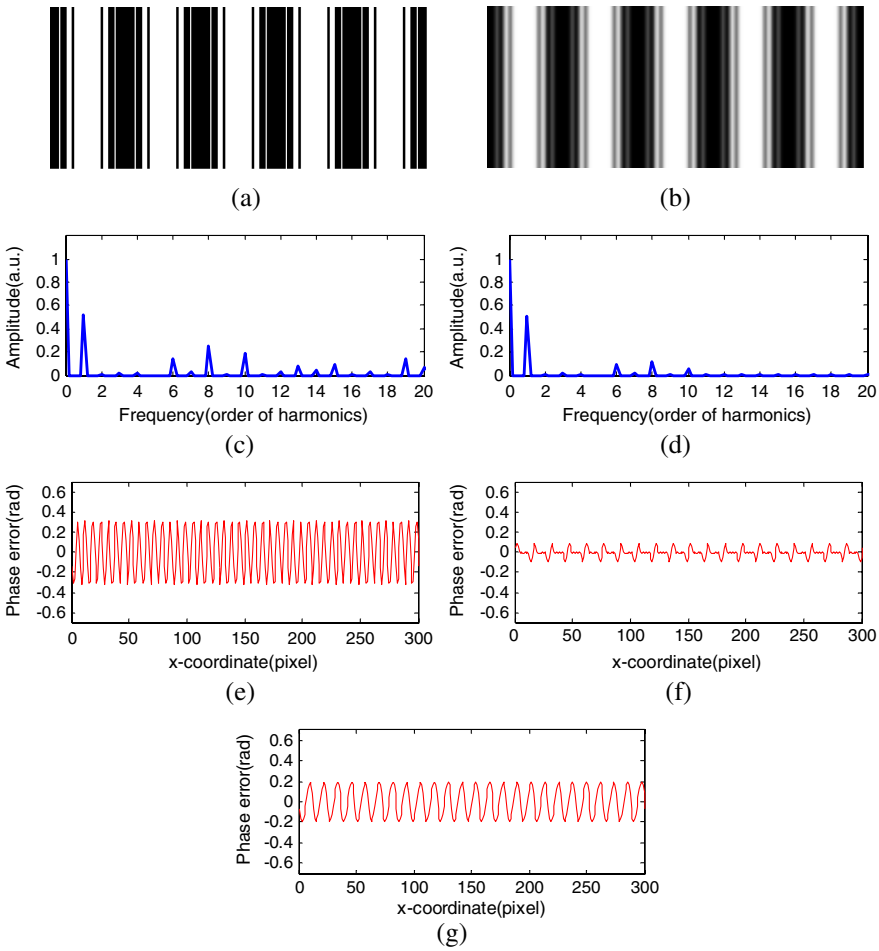

Fig. 11. (Color online) Simulation results of SPWM ($f_c = 8f_0$) using three to five-step phase-shifting algorithms. (a) The original SPWM pattern; (b) the Gaussian smoothed version of (a); (c) frequency spectrum of (a); (d) frequency spectrum of (b); (e) the phase error of three-step algorithm (RMS: 0.2319 rad); (f) the phase error of four-step algorithm (RMS: 0.0436 rad); (g) the phase error of five-step algorithm (RMS: 0.1396 rad).

verify the rationality of these results. The four-step algorithm resulted in the largest phase error, which was expected because it is sensitive to all odd-order harmonics. The phase error in the three-step method is much smaller since the third harmonics did not induce phase error in three-step algorithm. Due to its insensitivity to third-, fifth-, and seventh-order harmonics, the five-step method shows an even smaller RMS error—0.0697 rad.

Figure 11 shows the simulation results with the proposed SPWM plus four-step phase-shifting algorithm (f_c was chosen as $8f_0$). It can be seen, with a small defocusing level, that the spectrum of the pattern contained only three evident higher-order peaks, corresponding to the sixth-, eighth, and 10th-order harmonics. These three harmonics did not induce any phase error in the four-step algorithm but would affect the phase of three-step algorithm. The final phase errors shown in Figs. 11(e) and 11(f) met our expectations. The RMS error for the proposed SPWM plus four-step phase-shifting algorithm is only 0.0436 rad. This value is insignificant for most of the measurements. Although one more step of phase-shifting was used, the phase error of the five-step algorithm did not further improve due to the error derived from sixth-order harmonic.

Next we demonstrate the results of the SPWM patterns when f_c was chosen as $9f_0$ (Fig. 12). Similarly, there were three evident higher-order peaks, corresponding to the seventh, ninth, and 11th-order harmonics in the spectrum of the defocused pattern. But unfortunately, none of the three phase-shifting algorithms produced good result. The seventh-order harmonic induced phase errors in three- and four-step algorithms, the ninth-order harmonic induced phase errors in four- and five-step algorithms, and the 11th-order harmonics induced phase errors in all the three algorithms.

The simulation results with tripolar SPWM patterns (f_c was chosen as $8f_0$) are given in Fig. 13. We can see that the tripolar SPWM could generate high-quality sinusoidal patterns with a very small defocusing degree, and there was almost no evident high-order harmonics in the spectrum of the defocused pattern. Due the high sinusoidality of the tripolar SPWM pattern, all the three phase-shifting algorithms gave satisfactory results with almost the same level of phase errors as the SPWM plus

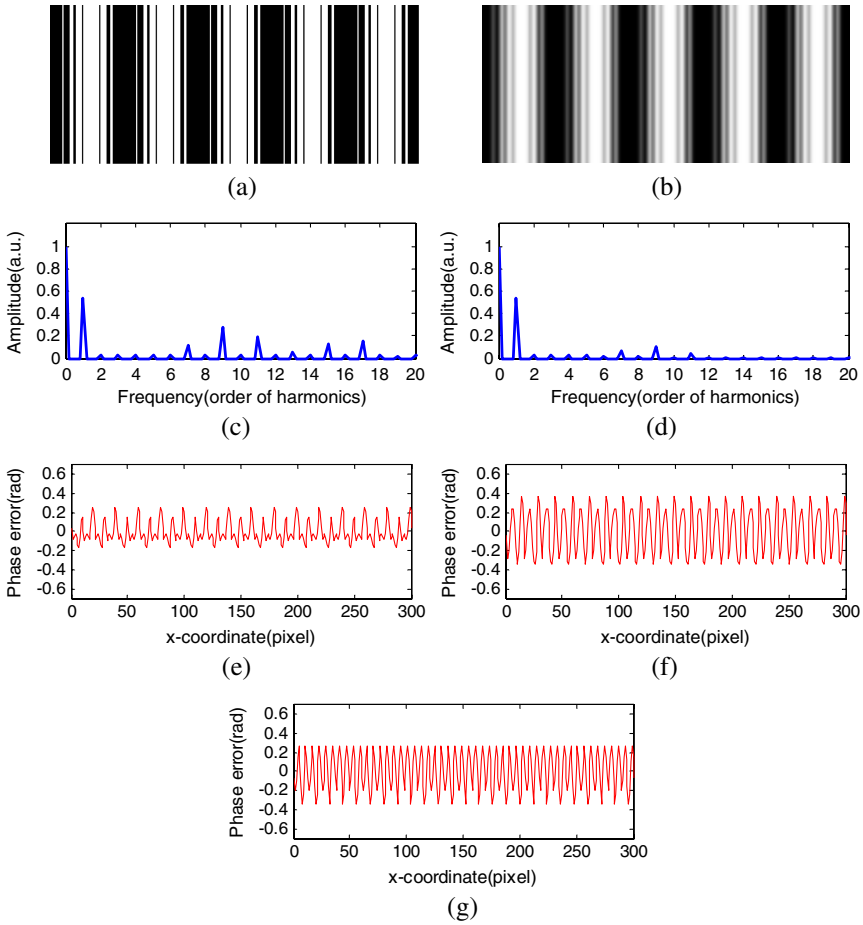

Fig. 12. (Color online) Simulation results of SPWM ($f_c = 9f_0$) using three to five-step phase-shifting algorithms. (a) The original SPWM pattern; (b) the Gaussian smoothed version of (a); (c) frequency spectrum of (a); (d) frequency spectrum of (b); (e) the phase error of three-step algorithm (RMS: 0.1135 rad); (f) the phase error of four-step algorithm (RMS: 0.2306 rad); (g) the phase error of five-step algorithm (RMS: 0.1986 rad).

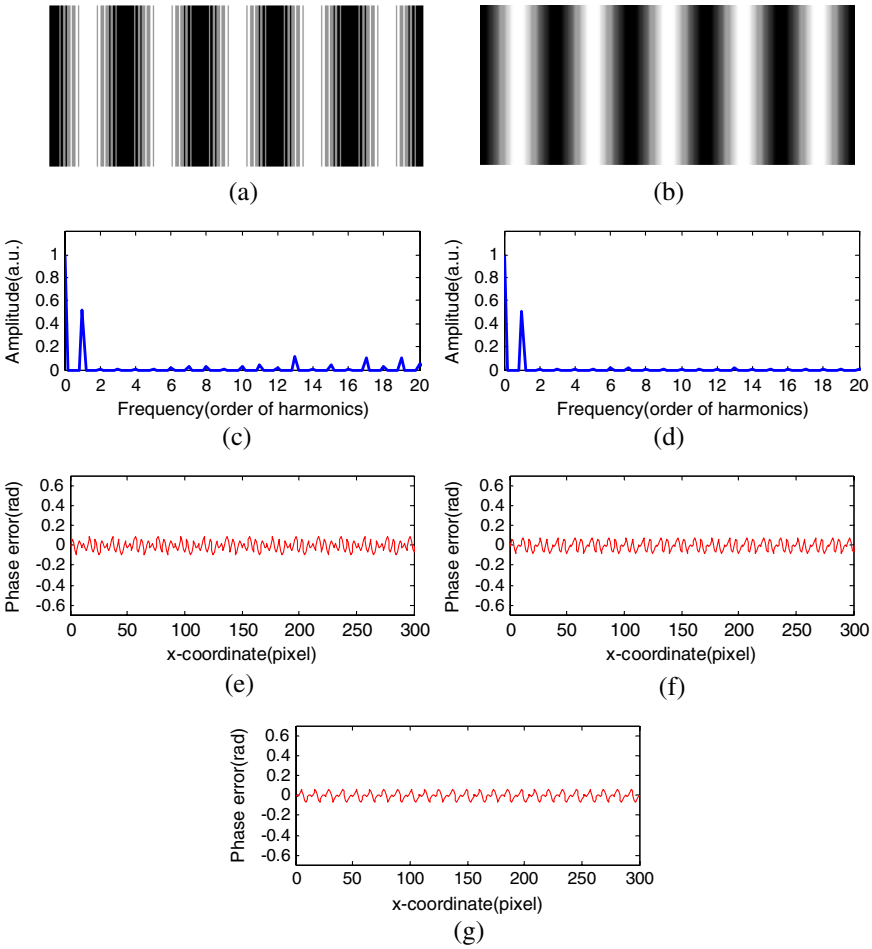

Fig. 13. (Color online) Simulation results of tripolar SPWM($f_c = 8f_0$) using three to five-step phase-shifting algorithms. (a) The original tripolar SPWM pattern; (b) the Gaussian smoothed version of (a) (filter size 8 pixels, standard deviation 1.5 pixels); (c) frequency spectrum of (a); (d) frequency spectrum of (b); (e) the phase error of three-step algorithm (RMS: 0.0488 rad); (f) the phase error of four-step algorithm (RMS: 0.0468 rad); (g) the phase error of five-step algorithm (RMS: 0.0389 rad).

four-step phase-shifting algorithm. The only difference is that the number of phase steps can be reduced from four to three when combined with the three-step algorithm, requiring one less frame.

It should also be mentioned that the proposed SPWM plus four-step phase-shifting algorithm and tripolar SPWM should have no phase error *theoretically* with a small defocusing level (equivalent to the effect of Gaussian filter in our simulations). Their phase errors are mainly due to some unwanted error-causing harmonics resulting from the discrete nature of the patterns; e.g., there was a very low peak corresponding to the third-order harmonics in the spectrum defocus SPWM pattern (f_c was chosen as $8f_0$). This effect of the discrete pattern can be minimized according to our proposed principles, but it cannot be eliminated completely.

5. Experiments

To further verify the proposed methods, a 3D shape measurement system was built comprising a DMD projector (X1161PA, Acer) and a CCD camera (GE680, Allied Vision Technologies) with a computer1614-MP lens $F/1.4$ with f of 16 mm. The resolution of the camera is 640×480, with a maximum frame rate of 205 frames per second. The projector has are solution of 800×600 with a lens of $F/2.41 - 2.55$ with of 21.79 mm–23.99 mm.

We first measured a simple geometry plaster model, comparing the results from different pattern schemes with three-, four-, and five-step phase-shifting algorithms. The patterns used were same as those in our previous simulations. The digital video projector projected those fringe patterns, and the CCD camera captured the reflected fringe images with the tested plaster model. In this experiment, the projector was slightly defocused. To better visualize the defocusing level, we show the tested object with the different projected patterns in Figs. 14(a), 14(e), 14(i), and 14(m), respectively. The measurement results of three-, four-, and five-step phase-shifting algorithms using SBM patterns are shown in Figs. 14(b), 14(c), and 14(d), respectively. The three- and four-step algorithms produced results with clearly noticeable ripples, while the error in the five-step algorithm was much smaller but still

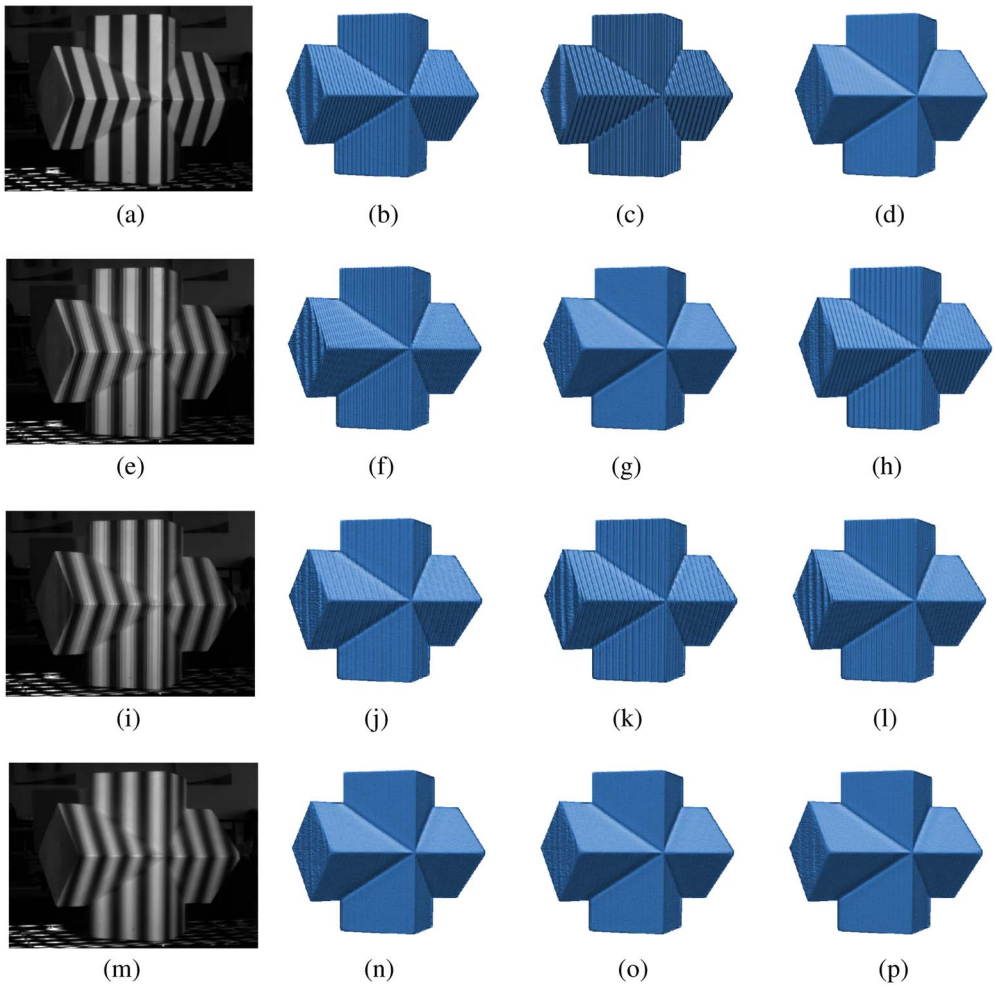

Fig. 14. (Color online) 3D measurement results of a plaster geometric model using different patterns (fringe pitch 60 pixels) with different phase-shifting algorithms when the projector is slightly defocused. The first row shows the tested object with SBM pattern (a), the 3D results of three-, four-, and five-step phase-shifting algorithms using SBM patterns (b)–(d). The second row shows the tested object with SPWM pattern ($f_c = 8f_0$) (e), the 3-D results of three-, four-, and five-steps phase-shifting algorithms using SPWM patterns ($f_c = 8f_0$) (f–h). The third row shows the tested object with SPWM pattern ($f_c = 8f_0$) (i), the 3D results of three-, four-, and five-steps phase-shifting algorithms using SPWM patterns ($f_c = 9f_0$) (j)–(l). The forth row shows the tested object with tripolar SPWM pattern ($f_c = 8f_0$) (m), and the 3D results of three-, four-, and five-step phase-shifting algorithms using tripolar patterns ($f_c = 8f_0$) (n-p).

noticeable. From the results of SPWM with $f_c = 8f_0$ [Figs. 14(f)–14(h)], we can see that the five-step algorithm produces weaker and lower-frequency corrugations than the three-step algorithm, and the four-step method generates the best 3-D shapes, in which the ripples are hardly noticeable. Using SPWM pattern with $f_c = 9f_0$, all the three phase-shifting methods generated harmonic-distorted 3D results [Figs. 14(j)–14(l)], but comparatively speaking, the result of the three-step method was smoother. When the tripolar SPWM patterns were applied, almost no regular ripples were noticeable in all results of different phase-shifting methods. The simulated and experimental results were in good agreement, which have verified the validity and rationality of the two proposed methods. We can conclude that if the main source of error is random noise in the pattern, then the proposed SPWM plus four-step phase-shifting algorithm and tripolar SPWM method can generate results with errors of small scale that are hardly comparable with the magnitude of the phase error due to the noise encoded in the fringe pattern.

To further validate the feasibility of the methods proposed in this paper, a more complicated plaster sculpture was also measured. The fringe pitch was chosen as 48 pixels, and we used $f_c = 6f_0$ for the SPWM pattern and $f_c = 7f_0$ for the tripolar SPWM pattern. Figures 15(a) and 15(c) show the five periods of one projected SPWM pattern and one tripolar SPWM pattern, respectively. Figures 15(b) and 15(e) show the tested object with distorted fringe patterns. It can be seen that the defocusing level was so small that the structure of the SPWM pattern can be clearly identified. But even with this defocusing level, the ideal sinusoidal pattern could be generated by using our tripolar SPWM technique. We use the four-step method for SPWM patterns and the three-step method for tripolar SPWM patterns. The final measurement results were shown in

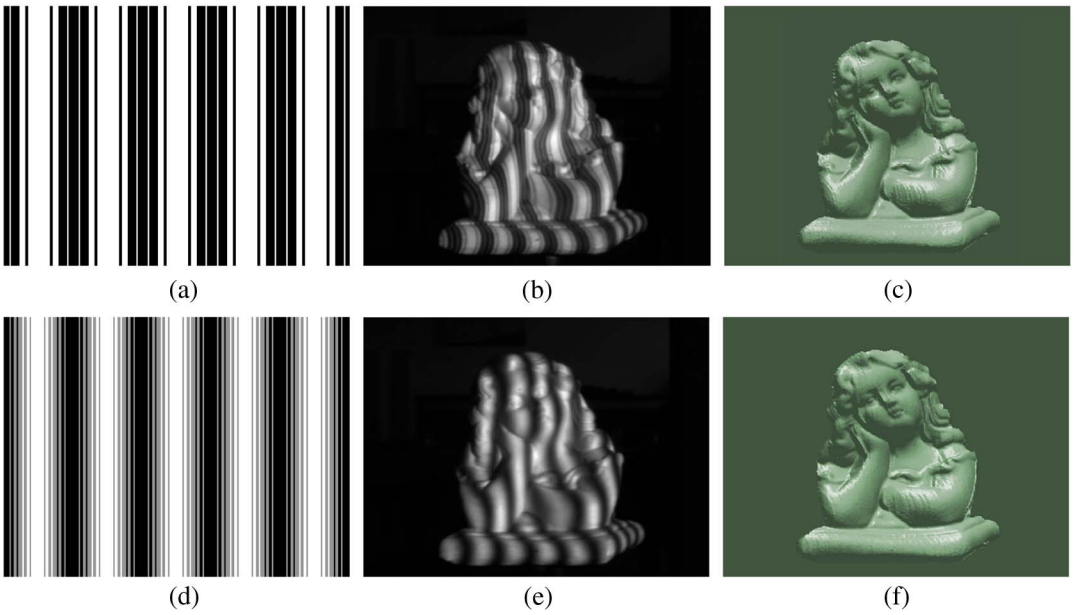

Fig. 15. (Color online) 3D shape measurement of a complex sculpture using the proposed techniques (fringe pitch 48 pixels). (a) One of SPWM pattern with $f_c = 6f_0$; (b) the measured object with the slightly defocused SPWM pattern; (c) 3D result with the SPWM plus four-step phase-shifting method; (d) one of tripolar SPWM pattern with $f_c = 7f_0$; (e) the measured object with the slightly defocused tripolar SPWM pattern; (f) 3D result with the tripolar SPWM plus three-step phase-shifting method.

Figs. 15(c) and 15(f). The 3D shape of the sculpture was faithfully reconstructed with the two proposed methods, resulting in smooth surfaces without spurious features. These results further confirmed that the proposed SPWM plus four-step phase-shifting algorithm and the tripolar SPWM method can success fully achieve accurate 3D measurement with a rather small level of defocusing.

6. Conclusions and Discussions

This paper has presented two techniques to minimize phase error and generate high-quality sinusoidal fringe patterns with projector defocusing to overcome the nonlinear response of the projector in a 3D shape measurement. We have analyzed the sensitivity of each harmonic frequency component affecting the calculated phase for different phase-shifting algorithms. Considering that the four-step phase-shifting algorithm is insensitive to all even-order harmonics, we have optimized the SPWM technique and combined it with the four-step phase-shifting algorithm. With this method, the dominant undesired harmonics can be shifted to higher even-order frequency so that they have no impact on the phase obtained by the four-step phase-shifting algorithm. The other method we have proposed is called tripolar SPWM, which uses one additional gray-level to further improve the SPWM method, modulating the undesired harmonics to very high frequencies. It can generate high-quality sinusoidal fringe pattern seven with a nearly focused optical system. Our simulation and experiment results have verified the validity of the proposed methods, showing that the remaining phase error is negligible for most applications. Besides, the improvement in performance is not at the cost of reducing the measurement speed (SPWM plus four-step phase-shifting algorithm only needs four patterns, and the triplor SPWM method combined with three-step phase-shifting algorithms only use three patterns) or involving additional postprocessing procedures. So our methods are very advantageous for real-time measurement in a time critical environment.

It may be worth noting that our methods may fail due to the nonlinear distortions of the CCD camera used in the measurement system. This may happen when the "gamma-correction" or "automatic gain control" (AGC) of the camera fails to be disabled. However, according to Pan *et al.* [20] and our experiential results, nonlinearity of the camera can be neglected compared to that of the projector in most cases. Another key issue to justify our work is that our pattern strategy employs only very few gray-levels (two or three), which is preferable for high-speed (kHz) applications since the DMD is a binary digital device. Because the DMD mirrors can be either on or off, a gray-scale image is created with the *binary temporal pulse width modulation* [21], and the intensity level is reproduced by controlling the amount of time the mirror is on/off. The fewer gray-scales the pattern is encoded, the fewer cycles are needed for DMD to recompose the pattern signals. So the proposed techniques have great potential for high-speed (kHz) shape measurement with higher accuracy and wider measurement depth range. This topic will be considered in our future work.

This work was supported by the Research and Innovation Plan for Graduate Students of Jiangsu

Higher Education Institutions, China (grant No. CXZZ11_0237).

References

1. F. Chen, G. M. Brown, and M. M. Song, "Overview of three-dimensional shape measurement using optical methods," Opt. Eng. **39**, 10–22 (2000).
2. S. S. Gorthi and P. Rastogi, "Fringe projection techniques: whither we are?," Opt. Lasers Eng. **48**, 133–140 (2010).
3. X. Y. Su and Q. C. Zhang, "Dynamic 3-D shape measurement method: a review," Opt. Laser Eng. **48**, 191–204 (2010).
4. S. Zhang, "Recent progresses on real-time 3D shape measurement using digital fringe projection techniques," Opt. Laser Eng. **48**, 149–158 (2010).
5. K. Liu, Y. C. Wang, D. L. Lau, Q. Hao, and L. G. Hassebrook, "Gamma model and its analysis for phase measuring profilometry," J. Opt. Soc. Am. A **27**, 553–562 (2010).
6. T. Hoang, B. Pan, D. Nguyen, and Z. Y. Wang, "Generic gamma correction for accuracy enhancement in fringe-projection profilometry," Opt. Lett. **35**, 1992–1994 (2010).
7. B. Pan, Q. Kemao, L. Huang, and A. Asundil, "Phase error analysis and compensation for nonsinusoidal waveforms in phase-shifting digital fringe projection profilometry," Opt. Lett. **34**, 416–418 (2009).
8. G. A. Ayubi, J. M. Di Martino, J. R. Alonso, A. Fernandez, C. D. Perciante, and J. A. Ferrari, "Three-dimensional profiling with binary fringes using phase-shifting interferometry algorithms," Appl. Opt. **50**, 147–154 (2011).
9. S. Y. Lei and S. Zhang, "Flexible 3-D shape measurement using projector defocusing," Opt. Lett. **34**, 3080–3082 (2009).
10. P. S. S. Huang, C. P. Zhang, and F. P. Chiang, "High-speed 3-D shape measurement based on digital fringe projection," Opt. Eng. **42**, 163–168 (2003).
11. S. Zhang and P. S. Huang, "Phase error compensation for a 3-D shape measurement system based on the phase-shifting method," Opt. Eng. **46**, 063601 (2007).
12. S. Zhang and S. T. Yau, "Generic nonsinusoidal phase error correction for three-dimensional shape measurement using a digital video projector," Appl. Opt. **46**, 36–43 (2007).
13. G. A. Ayubi, J. M. Di Martino, J. R. Alonso, A. Fernández, J. L. Flores, and J. A. Ferrari, "Color encoding of binary fringes for gamma correction in 3-D profiling," Opt. Lett. **37**, 1325–1327 (2012).
14. X.-Y. Su, W.-S. Zhou, G. von Bally, and D. Vukicevic, "Automated phase-measuring profilometry using defocused projection of a Ronchi grating," Opt. Commun. **94**, 561–573 (1992).
15. G. A. Ayubi, J. A. Ayubi, J. M. Di Martino, and J. A. Ferrari, "Pulse-width modulation in defocused three-dimensional fringe projection," Opt. Lett. **35**, 3682–3684 (2010).
16. Y. J. Wang and S. Zhang, "Optimal pulse width modulation for sinusoidal fringe generation with projector defocusing," Opt. Lett. **35**, 4121–4123 (2010).
17. Y. Wang and S. Zhang, "Comparison of the squared binary, sinusoidal pulse width modulation, and optimal pulse width modulation methods for three-dimensional shape measurement with projector defocusing," Appl. Opt. **51**, 861–872 (2012).
18. B. W. Williams, ed., *Principles and Elements of Power Electronics* (Barry W Williams, 2006).
19. L. Ekstrand and S. Zhang, "Three-dimensional profilometry with nearly focused binary phase-shifting algorithms," Opt. Lett. **36**, 4518–4520 (2011).
20. J. H. Pan, P. S. Huang, and F. P. Chiang, "Color-encoded digital fringe projection technique for high-speed 3-D shape measurement: color coupling and imbalance compensation," Proc. SPIE **5265**, 205–212 (2004).
21. R. Hofling and E. Ahl, "ALP: Universal DMD controller for metrology and testing," Proc. SPIE **5289**, 322–329 (2004).